Journal of Colloid and Interface Science **253,** 353–366 (2002)
doi:10.1006/jcis.2002.8527

Drop Penetration into Porous Powder Beds

Karen P. Hapgood,*,[1] James D. Litster,* Simon R. Biggs,† and Tony Howes*

*Department of Chemical Engineering, University of Queensland, Brisbane, Queensland, Australia, 4072; and †Department of Chemistry, University of Newcastle, Callaghan, New South Wales, Australia, 2308

Received June 15, 2001; accepted June 6, 2002; published online August 27, 2002

The kinetics of drop penetration were studied by filming single drops of several different fluids (water, PEG200, PEG600, and HPC solutions) as they penetrated into loosely packed beds of glass ballotini, lactose, zinc oxide, and titanium dioxide powders. Measured times ranged from 0.45 to 126 s and depended on the powder particle size, viscosity, surface tensions, and contact angle. The experimental drop penetration times were compared to existing theoretical predictions by M. Denesuk *et al.* (*J. Colloid Interface Sci.* 158, 114, 1993) and S. Middleman ("Modeling Axisymmetric Flows: Dynamics of Films, Jets, and Drops," Academic Press, San Diego, 1995) but did not agree. Loosely packed powder beds tend to have a heterogeneous bed structure containing large macrovoids which do not participate in liquid flow but are included implicitly in the existing approach to estimating powder pore size. A new two-phase model was proposed where the total volume of the macrovoids was assumed to be the difference between the bed porosity and the tap porosity. A new parameter, the effective porosity $\varepsilon_{\mathbf{eff}}$, was defined as the tap porosity multiplied by the fraction of pores that terminate at a macrovoid and are effectively blocked pores. The improved drop penetration model was much more successful at estimating the drop penetration time on all powders and the predicted times were generally within an order of magnitude of the experimental results.

Key Words: **nucleation; granulation; drop penetration; imbibition; porous powder beds; effective porosity; pore size.**

1. INTRODUCTION

Granulation is the process of agglomerating fine powdery materials using a liquid binder to give larger granules. This can be achieved in a range of different processing equipment including drums, pans, fluid beds, and high shear mixers. It is an important process in a range of industries including agricultural chemicals, pharmaceuticals, mineral processing, food, and detergents.

Granulation is an example of *particle design*. We adjust *formulation properties* (properties of the feed powder and liquid binder) and *process parameters* to give granules with controlled attributes, particularly granule size distribution and porosity. Modern research in wet granulation aims to quantify these effects so that granulation continues to move from an art to quantitative engineering.

Wet granulation is complex. Many phenomena occur simultaneously in the granulator which will influence the granule attributes. We divide these into three groups (1):

- granule nucleation and binder distribution;
- granule consolidation and growth;
- granule attrition and breakage.

Consider the process of nucleation in the spray zone of a granulator as shown in Fig. 1. Drops are formed at the spray nozzle, from which they fall and impact the bed surface. The drop then penetrates the bed surface by capillary action to form a nucleus granule. If the drop is slow to penetrate the surface or the flux of drops on the surface is high, drops will overlap and coalesce, leading to a broad nuclei size distribution (2).

Ideal nucleation conditions occur when one drop produces one nucleus granule (*drop controlled nucleation*). Therefore, to able to predict conditions for good nucleation, we need to study:

1. the kinetics of drop penetration, largely controlled by *formulation properties*; and
2. the flux of drops onto the bed surface, controlled largely by *process parameters*.

This paper considers the first of these constraints. The second constraint has been investigated separately (2).

Studying the kinetics of drop penetration is a new approach to understanding nucleation. The key question to be answered is: What happens when a single drop of fluid is placed on a powder surface?

2. DROP PENETRATION

Imbibition of a single drop into a porous substrate depends on the structure of the substrate: the porosity, the size of the pores, the orientation of the pores, and the surface chemistry within the bed (6). A simple model based on a bundle of parallel cylindrical capillaries has been derived independently by two authors (6, 7). Both approaches apply the Washburn equation where wetting is driven by the capillary pressure and resisted

[1] To whom correspondence should be addressed. Current address: Merck & Co., Inc., WP78-110, P.O. Box 4, West Point, PA 19486. Fax: (215) 652-2821. E-mail: karen_hapgood@merck.com.

0021-9797/02 $35.00

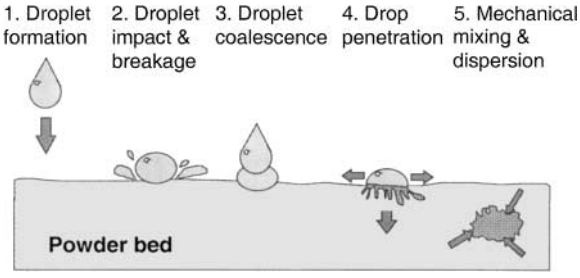

FIG. 1. The five steps of nucleation. 1, Droplet formation; 2, droplet impact on the powder and possible breakage; 3, droplet coalescence at the powder surface; 4, droplet penetration into the powder pores; 5, mixing of the liquid and powder by mechanical dispersion.

by viscous dissipation of the flow. The analysis considers only drop drainage.

The drop penetration time (also called the wicking time (6)) is defined as the time taken for the drop to penetrate completely into the porous substrate with no liquid remaining on the surface. In this paper, τ indicates a calculated penetration time and t_p indicates an experimentally determined penetration time.

Marmur (8) defines two limiting cases for the drop penetration behavior due to contact-angle hysteresis. The first case is the constant drawing area (CDA) case, where the three-phase contact line remains stationary (i.e., constant drop radius) and the apparent contact angle slowly decreases as the liquid drains from the droplet into the porous surface (see Fig. 2). This represents the fastest possible time for complete drop penetration, as the constant drawing area ensures that the number of pores available for drainage does not decrease. This is the most commonly used case and the drop penetration time under CDA conditions is given by (6, 7)

$$\tau_{CDA} = 1.35 \frac{V_o^{2/3}}{\varepsilon^2 R_{pore}} \frac{\mu}{\gamma_{LV} \cos\theta_d}, \quad [1]$$

where τ_{CDA} is the predicted penetration time for the constant drawing area case. Thus the penetration time depends on both wetting thermodynamics ($\gamma_{LV} \cos\theta$) and the wetting kinetics (strongly affected by μ and R_{pore}).

The second limiting case identified by Marmur (8) occurs when the apparent contact angle at the substrate surface remains constant throughout the penetration process and the liquid contact line retracts toward the center of the drop (see Fig. 2). This is the decreasing drawing area case (DDA) and represents the case where hysteresis of the contact angle is absent. It represents the upper penetration time limit because the number of pores underneath the droplet decreases as the drawing area decreases, slowing the drainage rate. The drop penetration time for the decreasing drawing area case, τ_{DDA}, is given by (see (7) for derivation)

$$\tau_{DDA} = 9\tau_{CDA}. \quad [2]$$

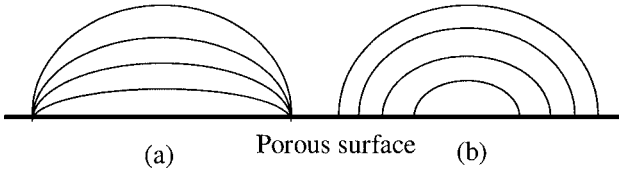

FIG. 2. Limiting cases of drop penetration on a porous surface proposed by Denesuk *et al.* (7). (a) Constant drawing area case. Constant drop radius and decreasing contact angle with time. (b) Decreasing drawing area case. Contact angle remains constant and the drop radius decreases with time.

These models of drop penetration are based on bundles of parallel cylindrical capillaries. Good experimental verification was obtained by placing drops of silicone oil on ordered porous substrates with parallel hexagonal pores (6, 7). However, there is very limited work on more complex powder bed systems and no observations have been recorded of the type of penetration (CDA or DDA).

The imbibition of water into glass ballotini and NaCl powder compacts of varying porosity has been studied (3). However, their interpretations of macroscopic contact angle are misleading (4) and their data is of limited use in this study. Recently, carbon black powder and six fluids with differing surface tensions and polarities were used to study the wetting of powders and compacts (5). Drop penetration time was one of the methods used to characterize the wetting behavior. A small drop of fluid was placed onto a compressed powder compact and the time taken for the drop to penetrate completely into the powder compact was measured using a CCD camera and an image analysis system. They suggested that the penetration time should be a function of the saturation and capillary number but no clear relationship was found. Although the contact angles of the fluids on the carbon black were measured using the sessile drop technique, no details of the results were given and the contact angle was not included in their proposed controlling group. However, their results showed that experimental penetration times could vary by over two orders of magnitude depending on the fluid properties. Since only carbon black was used in this study, the effect of changes in powder bed chemistry and packing structure are still unknown.

3. REVISED THEORY FOR LOOSELY PACKED POWDER BEDS

The main difficulty with the existing model (6, 7) is that the assumption of parallel capillary pores cannot be applied directly to powder beds. The Kozeny approach employed is commonly used in powder systems to define an effective pore size based on properties of the powder,

$$R_{pore} = \frac{2\varepsilon}{(1-\varepsilon) S_o \rho_s}, \quad [3]$$

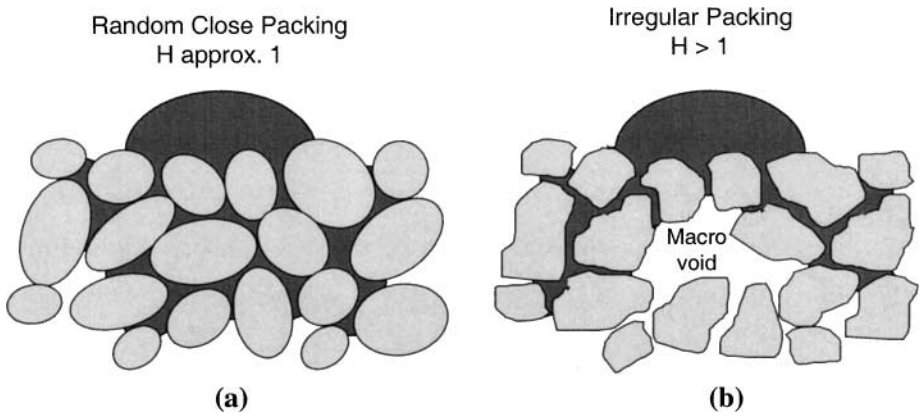

FIG. 3. (a) For close packing powders the fluid drainage is relatively uninhibited. (b) As liquid penetrates into powders containing large macrovoids the liquid front will tend to halt when the pore radius increases suddenly. This occurs whenever a capillary pore reaches a macrovoid. The macrovoid space does not contribute to the effective capillary volume or surface area.

where S_o is the particle specific surface area expressed in m^2/kg. Equation [3] relates the estimated pore diameter to measurable quantities of the powder bed—the porosity and the specific surface area of the particles.

An alternative approach is to assume the particles are approximately spherical. The surface mean particle diameter d_{32} is defined as the diameter of a sphere with the same surface to volume ratio as the irregular particle. Therefore, the d_{32} particle size together with a shape factor ϕ (which accounts for nonspherical particle shape) can be used in [3] instead of the specific surface area resulting in the following expression relating particle size to pore size:

$$R_{\text{pore}} = \frac{\phi d_{32}}{3} \frac{\varepsilon}{(1-\varepsilon)}. \qquad [4]$$

A third approach is to model the pore structure as an assembly of parallel, cylindrical capillaries of varying radius (9). This approach is difficult to apply to powder beds and will not be considered here.

The Kozeny approach to estimating the pore size of powder beds assumes well-packed pores and a homogeneous bed structure. It has been successfully used to describe fluid flow through beds of *well-packed particles*, such as soils, filtration, or when a driving pressure is being applied to the liquid (mercury porosimetry). However, powder in a granulator is in motion and extremely loosely packed and the existing model is unlikely to characterize the powder bed structure. A new drop penetration time model for loosely packed powder is required to model drop imbibition in a granulator.

Liquid penetration into the powder pores is driven by surface tension, contact angle and pore radius. The liquid will advance into the powder by flowing down successively smaller pores. As the pore widens the surface curvature of the fluid will reduce and the fluid velocity will slow. Eventually a pore may widen so that the surface curvature of the liquid disappears and fluid ceases to advance along the pores. Ideally, fluid imbibition requires either *equisized* or *monotonically decreasing* pore radii. In practice, a narrow distribution of pore sizes will permit fluid imbibition. However, heterogenous pore size distributions will contain pores which suddenly widen due to the presence of large macrovoids. The sudden widening will halt fluid flow and *all pores that open into a void with a much larger radius than the pore are effectively blocked*. This is illustrated in Fig. 3.

Equations [3] and [4] estimate the powder pore size by dividing the void volume by the void surface area. The powder in a granulator is in motion and the local powder bed and pore structure will be heterogeneous and will contain large "bubble voids" or macrovoids (10, 11). When the Kozeny approach is applied to loosely packed beds of irregular or cohesive particles, ε includes the contribution of macrovoids which do not participate in liquid flow.

The problem with including macrovoid space when calculating pore size is illustrated in Fig. 4. As liquid infiltrates a pore with an initial radius R that suddenly widens to a radius $2R$, the liquid stops at the opening of the larger void space. However, [3] and [4] include the void space of the wide neck, even though it does not participate in liquid drainage, and incorrectly estimates the effective pore size as $1.5R$. In addition, [3]

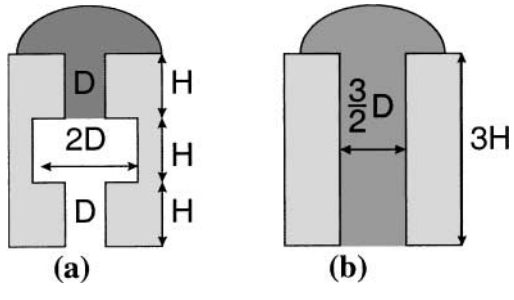

FIG. 4. (a) The presence of sudden large pore openings in actual pores leads to misleading R_{pore} estimations (b) when the Kozeny approach is used.

and [4] do not predict the effective blockage of the fluid path. Similar issues exist in interpreting mercury porosimetry results (10).

The Hausner ratio is the ratio of the actual porosity to the tap porosity and partially describes the packing state of the powder (12):

$$H = \frac{\varepsilon}{\varepsilon_{\text{tap}}}. \quad [5]$$

The Hausner ratio characterizes the interparticle friction. When the Hausner ratio $H \approx 1$ the Kozeny equation should be valid as there should be very few macrovoids. Smooth glass ballotini spheres can be expected to have a low Hausner ratio and their pores should be consistent with the Kozeny equation. However, as H increases the likelihood of large macrovoids forming increases.

We propose a new, simple "two-phase" model for powder packing in loosely packed powder beds. Consider a powder at its tap density. It is assumed that no macrovoids are present when $\varepsilon = \varepsilon_{\text{tap}}$. As the porosity of the powder is increased above ε_{tap}, random close packing conditions begin to break down and macrovoids begin to form. As the powder voidage increases further we assume the extra voidage contributes exclusively to the formation of macrovoids:

$$\varepsilon_{\text{macrovoids}} = \varepsilon - \varepsilon_{\text{tap}}. \quad [6]$$

This is analogous to the excess fluidization gas forming bubbles used in two-phase models for fluidized beds (13). This also implies that ε_{tap} is approximately equal to the volume of pores which are capillaries suitable for liquid drainage.

The effective porosity of the bed could be taken as ε_{tap}, but a proportion of capillary pores will terminate at a macrovoid and hence do not participate any further in fluid drainage. The liquid must seek other smaller pores to go around the macrovoid. Therefore, ε_{tap} is multiplied by the fraction of pores that participate in drainage. The fraction of pores that terminate at a macrovoid is assumed to be proportional to the volume of macrovoids and the new effective porosity is defined as:

$$\varepsilon_{\text{eff}} = \varepsilon_{\text{tap}}(1 - \varepsilon_{\text{macrovoids}}) = \varepsilon_{\text{tap}}(1 - \varepsilon + \varepsilon_{\text{tap}}). \quad [7]$$

This effective porosity is substituted into [3] and [1] as follows:

$$R_{\text{eff}} = \frac{\phi d_{32}}{3} \frac{\varepsilon_{\text{eff}}}{(1 - \varepsilon_{\text{eff}})} \quad [8]$$

$$\tau_{\text{CDA}} = 1.35 \frac{V_{\text{o}}^{2/3}}{\varepsilon_{\text{eff}}^2 R_{\text{eff}}} \frac{\mu}{\gamma_{\text{LV}} \cos\theta_{\text{d}}}. \quad [9]$$

Equation [2] for τ_{DDA} remains unchanged.

Three possible equations for estimating R_{pore} have been presented:

1. Eq. [3] with S_{o} equal to the particle specific surface area;
2. Eq. [4] using ϕd_{32};
3. Eq. [8] for R_{eff} using ε_{eff}.

This paper describes a series of experiments to test the existing and new, two-phase models for drop penetration time using a broader range of variables and a more complex system than has been studied previously. The ultimate goal is to determine the best method of estimating drop penetration time and nuclei formation kinetics in a granulator.

4. MATERIALS AND METHODS

4.1. Materials Characterization

Several different powders and binders were selected so that a range of material properties were covered. Two sizes of closely sized glass ballotini spheres (Potters Industries, Laverton, Australia) were used: fine AI ballotini with $d_{43} = 35$ μm and coarser AE ballotini with $d_{43} = 160$ μm. Two different lactose monohydrate powders with different size distributions were used. The first was manufactured by Wyndale New Zealand Milk supplied through the University of Queensland and referred to in the paper as "UQ lactose." This lactose was also sieved into three narrow size fractions: "fine lactose," 45–106 μm; "medium lactose," 106–180 μm; and "coarse lactose," 180–250 μm. A second grade of lactose supplied by Merck & Co., Inc., (manufactured by Foremost Farms, USA; referred to as "Merck lactose") had a smaller and narrower particle size distribution than UQ lactose. Experiments were also performed on zinc oxide and titanium dioxide which are very fine and cohesive powders.

Powder properties are summarised in Table 1. Particle size distributions were measured using a Malvern Mastersizer/E.

TABLE 1
Powder Properties Summary

	Glass ballotini		Lactose			
Powder property	AI	AE	UQ	Merck	ZnO	TiO_2
Surface mean d_{32} (μm)	29.61	113.4	64.43	17.86	1.25	0.73
Volume mean d_{43} (μm)	34.81	160.7	168.7	69.2	2.55	2.79
d_{10} (μm)	21.52	72.48	38.97	7.8	0.61	0.30
d_{50} (μm)	32.56	119.9	138.2	64.8	1.73	1.21
d_{90} (μm)	50.56	328.4	348.3	131.2	5.19	5.98
True particle density (g/cm^3)	2.463	—	1.536	1.54[a]	5.86	4.17
Tap density (g/mL)	1.50	1.54	0.935	0.93[a]	2.3[b]	1.7[b]
BET specific surface area (m^2/kg)	158.3	85.9	—	—	4499	1537
Malvern specific surface area (m^2/kg)	79.7	20.8	60.5	—	817	1965

[a] Data from Mackaplow *et al.* (24).
[b] True tap density conditions estimated by powder compaction technique.

Standard optical presentation factors were used for all powders except for ZnO and TiO_2, which used optical corrections 1807 and 2207, respectively. To prevent dissolution of the lactose during measurement, the dispersing fluid used was a saturated 95% ethanol solution. All other powders were dispersed in water. The true density of the particles was measured using a helium picnometer (Micromeritics Accupyc 1330). Tap density was determined in a 25-mL cylinder using a 3-mm stroke for 3000 taps following ASTM B527-93. Note that air voids were still visible after extensive tapping of the ZnO and TiO_2 powders and true tap density was not achieved. A powder compaction curve was used to estimate the tap density of these fine powders.

The BET surface area of glass spheres, ZnO, and TiO_2 were measured using nitrogen gas adsorption (Gemini 375). The surface area of the lactose powder could not be measured accurately as the sample preparation method dramatically affected the results. Desiccation and drying the sample results in dehydration of the lactose which in turn alters the crystal structure and surface area (14).

Six different binder fluids were used: water, two polyethylene glycol binders with molecular weights of 200 and 600 (PEG200 and PEG600, respectively), two solutions of hydroxypropyl cellulose (HPC) (3.5 and 7 wt%) and a 0.00094 M NDBS solution.

A 7 wt% HPC solution was prepared by slowly dissolving 70 g of HPC in 930 g of cold water. The solution was left to stir overnight and covered in foil to minimize evaporation. Liquid properties were measured the following day. To prepare a lower viscosity HPC solution, the original HPC solution was diluted 1 : 1, creating a 3.5 wt% solution with a viscosity of 17.3 cP. The NDBS solution was prepared for a previous project (15).

A summary of binder properties is given in Table 2. Viscosity and surface tension measurements were performed in duplicate and an average result is shown in Table 2. Surface tension was measured using the Wilhelmy plate technique, and viscosity was measured using either a constant-stress rheometer or a Brookfield DV-III rheometer. For some experiments, red dye was added to assist binder fluid visibility. Properties of these solutions are shown with and without the dye. The dye reduced the surface tension of the solution by a very small amount.

TABLE 2
Binder Fluid Properties

Binder fluid	Density ρ_L (g/mL)	Surface tension γ_L (mN/m)	Viscosity μ (mPa · s)
Water	1	72.1	1.1
Water and red dye	1.0129	70.55	1.1[b]
Saturated lactose solution	1.071[a]	71.6[a]	1.1[b]
3.5 wt% HPC and red dye		42.25	17.3
7 wt% HPC	1.0139	42.25	103.7
7 wt% HPC and red food dye	1.0139	42.28	104.0
PEG200	1.127	43.7	63.8
PEG600	1.128	43.7	152.9
NDBS	1[b]	31[c]	1.1[b]

[a] Data from (24) and (20).
[b] Assumed to be indentical to that of water.
[c] Data from (14).

TABLE 3
Contact Angles Results Measured by the Opposing Air Pressure Technique

Powder	Grade	Fluid	Measured wetted S_o (m^2/kg)	θ (°)	θ_{LIT} (°)	References
Glass ballotini	AI	Water	65 ± 10	52 ± 14	44[a]–60[b]	*a* (23)
		NDBS	65 ± 10	52 ± 1		*b* (25)
		PEG200	65 ± 10	65 ± 6		*c* (26)
		PEG600	65 ± 10	68 ± 6		*d* (20)
	AE	Water	16 ± 3	58 ± 1	44[a]–60[b]	*e* (21)
		PEG200	16 ± 3	67 ± 5		*f* (27)
Lactose	UQ	Saturated solution	50 ± 25	63 ± 9	30[c,d], 62[j], 74[e]	*g* (28)
		NDBS	50 ± 25	64 ± 7		*h* (29)
		PEG200	50 ± 25	64	56[e]	*i* (30)
	Merck	5% HPC			34[g]	*j* (22)
ZnO		Water		—	32[h]	
TiO_2		Water		—	70[i]	

Note. Numbers are the mean and the standard deviation of all successful results.

The interfacial properties of most powder/binder combinations were measured using the opposing pressure technique (16), where the air pressure required to halt the advancing liquid front in a packed powder column is recorded. The opposing air pressure method has been successfully used to measure contact angles of several powders (17, 18), including complex heterogeneous powders (19). The contact angle is calculated by comparing the capillary pressures of two different fluids, one of which has a known contact angle. The technique assumes that the macroscopic wetting front is large in comparison to the individual particles. When this condition is met the measured pressure difference is a statistical average over a large number of particles differing in their individual specific surface energies. The technique is generally suitable for particles in the size range 25 to 300 μm (17, 18). Advancing contact angle measurements were performed using the same equipment and procedure as Iveson *et al.* (19). Experimental results are summarized in Table 3.

All of the contact angles measured by the opposing air technique are quite high and fall between 52 and 88 degrees. There is reasonable agreement between the literature data and opposing pressure results. The manufacturing process, storage conditions, degree of cleaning, and measurement technique all introduce variation into the expected results. All powders used in this work were used "as received" and no special surface cleaning

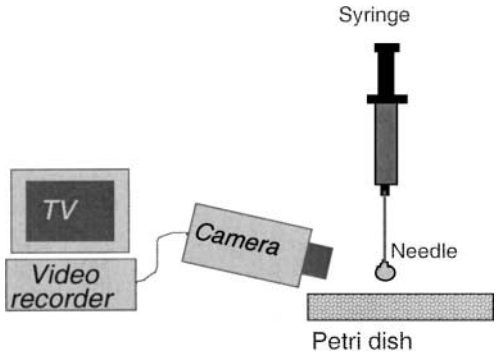

FIG. 5. Schematic diagram of drop penetration experimental setup.

or preparation was used. The lower contact angles for water on glass ballotini were measured on cleaned ballotini (24) and the uncleaned contact angle would be expected to be higher. Several papers using several different methods (20–23) quote the contact angle of water or a saturated lactose solution on lactose powder to be 30°, although other studies (22, 23) suggest higher values. This work suggests that the contact angle of a saturated lactose is 63°, which is significantly higher than the popularly accepted 30° but within the range of literature values.

4.2. Drop Penetration Time Measurement Technique

A schematic diagram of the drop penetration measurement apparatus is shown in Fig. 5. A loosely packed bed was considered to be the best approximation to conditions experienced by the powder in a granulator which is agitated either mechanically or by fluidizing air. The dish was 85 mm in diameter and 17.4 mm deep, which was sufficient to avoid interfering with the drainage process (3–4 drop diameters deep). A loosely packed powder bed was formed by lightly sieving the powder through a 250-μm sieve into a petri dish and scraping level with a metal spatula to produce a smooth powder surface. Although the scraping procedure may affect the local porosity at the powder surface, this would be a minor effect compared to the heterogeneous pore structure of the entire powder bed. The weight of powder added to the dish was recorded to calculate average porosity.

A 100-μL SGE syringe with a 25-gauge needle was positioned just above the bed surface. This allowed the drop to fully detach from the needle but minimized the height of the fall. Relatively large nuclei granules were formed because the drop size was much larger than is typical from a spray nozzle. Red or blue dye was added to the binders to assist drop visibility. The drop size of each fluid was estimated at the end of each set of experiments by recording the volume of liquid added using the syringe markings or the mass of liquid added and dividing by the number of drops. The drop sizes varied by approximately 1 μL for most fluids, with water varying by 2–3 μL as it was the most difficult fluid to dispense evenly by hand. Preliminary experiments verified that the addition of the dye did not affect the drop penetration times within experimental error.

A Zeiss Stemi 2000 microscope with a Sony CCD camera and a JVC SVHS video recorder operating at 25 frames/s were used to film a single drop of binder penetrating into the powder surface. A spotlight was used to illuminate the powder bed beneath the drop. The spotlight was turned off between runs to minimize radiant heating of the syringe fluid which might change the binder properties (see Fig. 6).

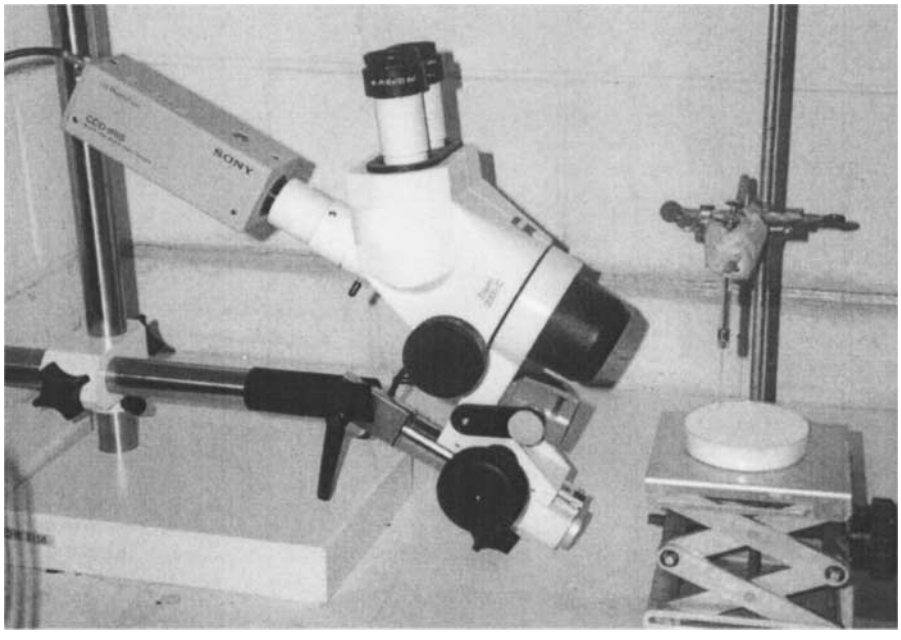

FIG. 6. Photograph of the drop penetration time experimental apparatus.

TABLE 4
Powder and Binder Combinations Used in Drop Penetration Experiments

Fluid	Water	PEG200	PEG600	NDBS solution	3.5% HPC	7% HPC	Lactose solution
AI ballotini	√	√	√	√			
AE ballotini	√	√					
Lactose (UQ)	√	√	√	√			√
Lactose (fine)	√	√					
Lactose (medium)	√	√					
Lactose (coarse)	√	√					
Lactose (Merck)	√				√	√	
Zinc oxide	√	√					
Titanium dioxide	√						

At least 15 replicates were performed for each binder. A number of runs were performed on each dish of powder. Each drop was at least 1 cm from the walls of the petri dish and neighboring drops. For fast penetrating drops, the penetration time was calculated from the video recording and taken as the number of frames between when the drop hit the powder surface and when the last liquid drained away. For slow-penetrating drops (20 s or more) a stopwatch was used as the changes in volume frame by frame on the video were too small to detect the end point. The end point was instead determined by eye using light reflections. As long as a fluid drop is present, a single light source will present a single reflection. Once the fluid drains below the powder surface, the light will be reflected from the rough powder surface and one light source produces several reflections. The appearance of multiple reflections was taken as the point at which drainage was complete.

The powder packing conditions in the petri dish were altered to study the effects of packing, porosity, and pore size, which are all closely interrelated. A packed bed was formed by sieving the powder through the 250-μm sieve and pressing the powder firmly into the petri dish. The effects of the particle size distribution were also investigated by sieving the UQ lactose into three size fractions: fine (45–106 μm), medium (106–180 μm), and coarse (180–250 μm). This provided three powders with identical properties except for particle size distribution and therefore packing characteristics.

Table 4 summarizes the combinations of powders and binders used to investigate drop penetration time behavior. The results from all experiments are discussed below.

5. RESULTS AND DISCUSSION

Figures 7 to 10 shows a series of images taken from the video footage of typical drop penetration behavior for several fluids on AI ballotini and Merck lactose powder. Only constant drawing area behavior was observed for all fluids on all powders—decreasing drawing area behavior does not seem to be applicable to liquid imbibition into porous powder beds. Therefore Eq. [2] cannot be used to describe drop penetration times into porous powder beds. This implies that contact angle hysteresis commonly occurs on powder surfaces.

A summary of the experimental penetration results are given in Table 5. Each value is the average of between 6 and 25 measurements. The average voidage (ε) and drop volume (V_o) of each experiment are also shown. The final column gives the mean measured time (t_p) and the standard error of the mean (95% confidence interval). The results in Table 5 confirm that drop penetration time can vary widely—from a minimum of 0.45 s for water on AI glass ballotini to 126 s for 7% HPC solution on Merck lactose. This agrees with other work (5) where t_p on carbon black powder varies by more than two orders of magnitude depending on the fluid properties.

5.1. *Effect of Fluid Properties on t_p*

The effect of liquid properties on drop penetration time can be predicted quite accurately. Figure 11 shows the experimentally determined mean drop penetration time for each powder plotted against the liquid properties group $\mu/\gamma \cos\theta$, derived from Eq. [1]. Each symbol represents a different powder and each point on the line represents a different fluid on that powder. The error bars show the 95% confidence interval of the mean. The confidence limits on the liquid properties group can be fairly large depending on the value of the contact angle and the

TABLE 5
Drop Penetration Time Results Summary

Powder	Fluid	n	ε (−)	V_o (μL)	t_p (s)	95% CI (s)
AI ballotini	Water	20	0.45	11.6	0.63	0.04
		20	0.42	8.5	0.45	0.06
	NDBS	6	0.52	8.3	0.65	0.12
	PEG200	23	0.49	5.7	6.9	0.6
		21	0.43	5.5	5.8	0.4
	PEG600	22	0.47	5.6	17.4	1.1
		20	0.40	5.7	18.6	2.7
AE	PEG200	7	0.38	6.9	3.0	0.2
UQ lactose	Water	21	0.61	9.0	0.67	0.05
		18	0.50	10.0	0.56	0.05
	Saturated solution	14	0.55	8.1	0.61	0.07
	NDBS	7	0.63	6.9	0.72	0.11
	PEG200	23	0.61	5.7	9.6	0.7
		20	0.48	6.3	10.7	0.9
	PEG600	21	0.59	5.7	21.7	1.1
		20	0.49	6.0	27.5	2.4
Merck lactose	Water	10	0.62	6.6	2.0	0.3
	Water and dye	25	0.59	5.9	2.2	0.11
	3.5% HPC and dye	20	0.61	4.4	21.5	1.1
	7% HPC	15	0.62	5.5	126	23
	7% HPC and dye	22	0.61	4.2	123	17.7
ZnO	Water	22	0.92	9.5	0.57	0.08
	PEG200	11	0.92	6.2	19.7	3.5
TiO_2	Water	13	0.84	9.8	8.7	1.2

Note. n = number of experiments, ε = bed porosity, V_o = drop volume, t_p = average penetration time, 95% CI = 95% confidence interval on the mean.

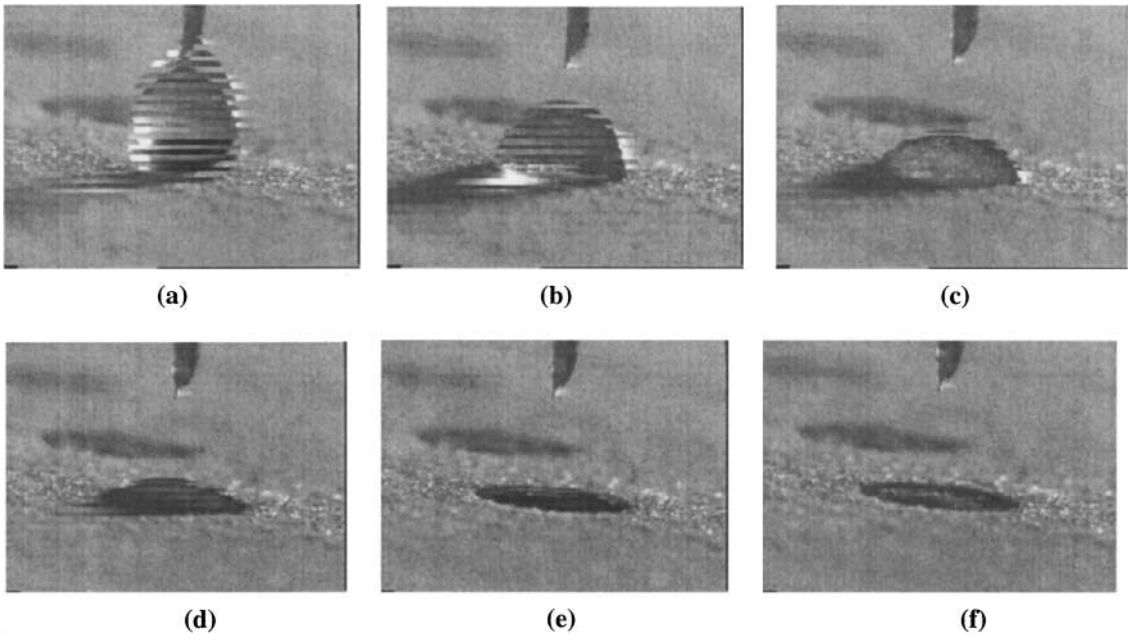

FIG. 7. Water on AI glass ballotini powder. The pictures are taken at (a) impact, (b) 0.07 s after impact, (c) 0.2 s, (d) 0.27 s, (e) 0.33 s, and (f) 0.4 s.

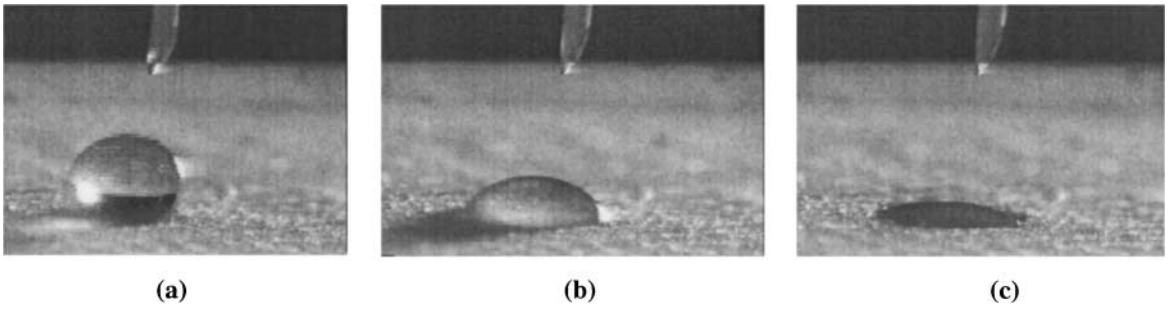

FIG. 8. Penetration of PEG200 into AI glass ballotini powder. The pictures are taken (a) just after impact, (b) 2 s after impact, and (c) 5.4 s after impact. The needle tip is visible in the top of the picture.

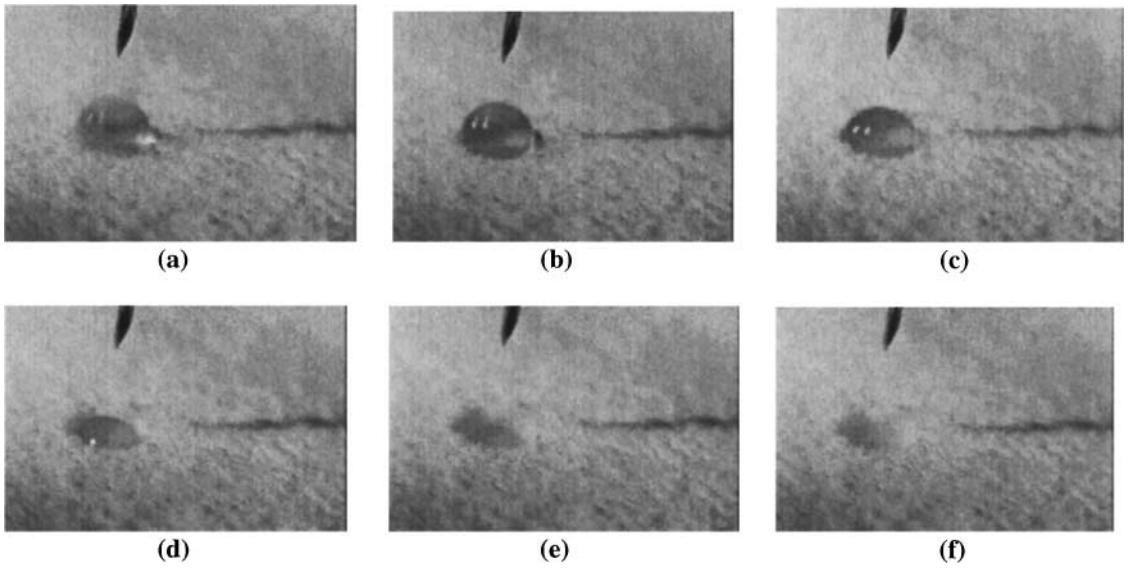

FIG. 9. Penetration of a water droplet on Merck lactose powder: (a) Impact, (b) 0.03 s, (c) 0.23 s, (d) 0.9 s, (e) 1.4 s, (f) 2.3 s.

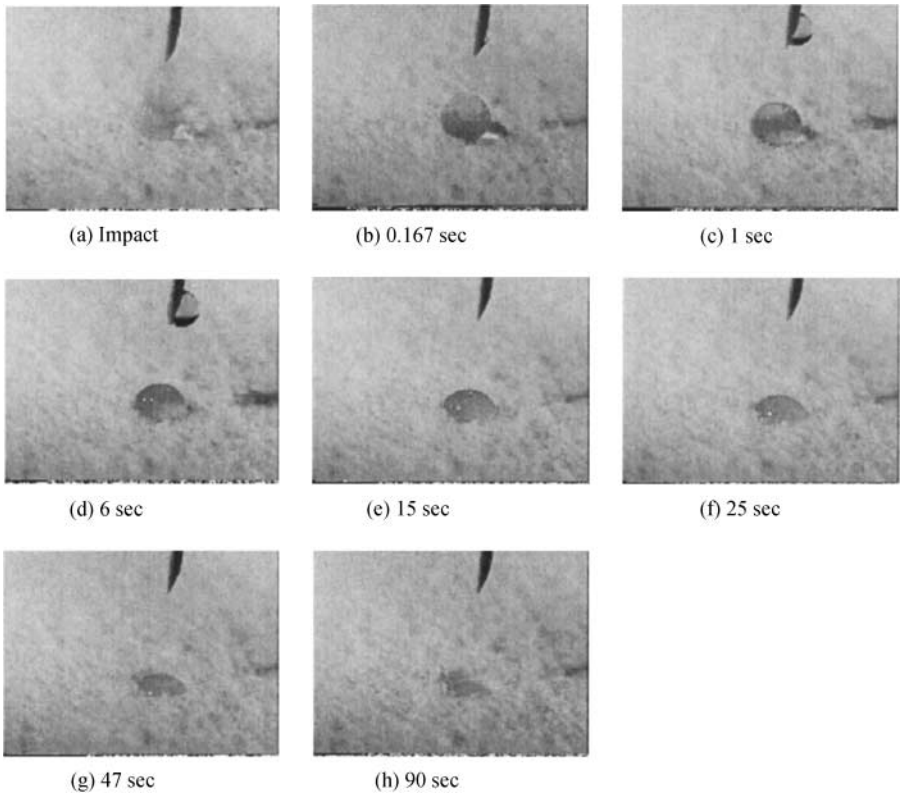

FIG. 10. Drop penetration sequence for 7% HPC solution on Merck lactose. Note that if the bed moved in the first second the drop would roll across the powder surface.

relative error (see Table 3). When the error on the contact angle was unknown it was assumed to be 20% or 10°, whichever was greater. Despite this, there is a linear relationship between the liquid property group $\mu/\gamma_{LV}\cos\theta$ and the penetration time for each powder. The lines do not all coincide because each powder has a different porosity and packing structure. The slope of each line represents approximately constant powder packing properties (ε, R_{pore}) for each powder and near constant initial drop size.

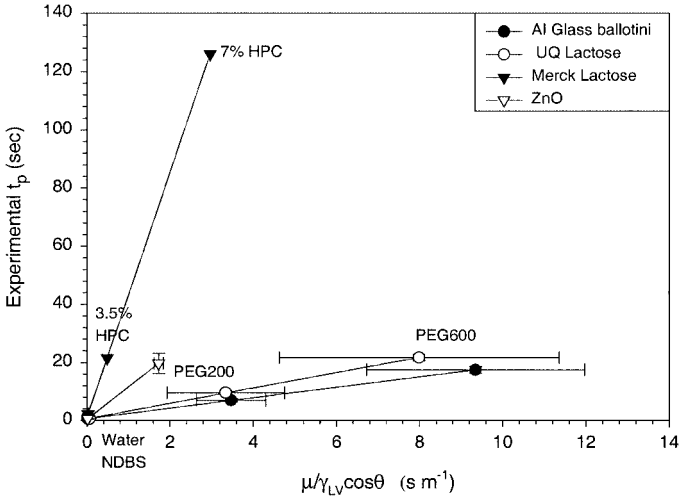

FIG. 11. Summary of the effect of liquid properties on t_p for all powders. Symbols represent mean penetration time for different powders (see legend) and each point on the line represents a different fluid as indicated. Error bars show the 95% confidence interval.

The penetration time is directly proportional to the viscosity and inversely proportional to the adhesion tension. Since binder viscosity can vary by 1–2 orders of magnitude it is the dominant influence on penetration time for a droplet of a given volume, provided that the contact angle is less than 90°.

Drop penetration times for water and a 0.0094 M NDBS solution were compared to investigate the role of surface tension. Water and NDBS were found to have the same contact angle on AI ballotini and UQ lactose, respectively (see Table 3), and have the same viscosity, but the NDBS has a surface tension of 31 mN/m, approximately half that of water (refer to Table 2).

Penetration time is expected to increase as γ_{LV} decreases, as reducing surface tension of the solution reduces the driving force ΔP_c for flow into the capillaries and slows the liquid velocity. This is predicted in the theoretical equation for penetration time [9] and was also reflected in the results. Since a reduced surface tension reduces both the capillary driving force and the drop volume produced by the needle, the raw results given in Table 5 show only a very small increase in penetration time. The decrease in drop volume approximately compensates for the slower fluid penetration and no significant effect of surface

TABLE 6
Effect of Surface Tension in Penetration Time

Powder	Fluid	γ_{LV} (mN/m)	n	ε (−)	t_p (s)	$t_p/V_o^{2/3}$ (s/μL$^{2/3}$)	95% CI (s/μL$^{2/3}$)
AI ballotini	Water	72	20	0.45	0.63	0.12	0.01
	NDBS	31	6	0.52	0.65	0.16	0.03
UQ lactose	Water	72	21	0.61	0.67	0.15	0.01
	NDBS	31	7	0.63	0.72	0.2	0.03

Note. See Table 5 for nomenclature.

tension was found using the raw data. However, Table 6 shows that when penetration time is normalized by the drop volume, $t_p/V_o^{2/3}$ from [1], the relative penetration time (per $\mu L^{2/3}$) of the NDBS solutions increases by a factor of 1/3 on both powders. An increase in $t_p/V_o^{2/3}$ due to a reduction in liquid surface tension is predicted by the theory, although the increase should be directly proportional to γ_{LV}. The discrepancy could be due to either the higher relative error when measuring short penetration times less than 1 s or due to degradation of the NDBS solution during storage.

The effect of fluid viscosity on the drop penetration time can be predicted accurately. Penetration time should be directly proportional to the fluid viscosity (see Eq. [1]). The ratio between PEG200 and PEG600 penetration times is almost identical to the ratio of their viscosities (see Table 7).

The results presented illustrate that the drop penetration model accurately describes the effects of the changing binder fluid properties (surface tension and viscosity) on the drop penetration time. For a given powder, the theory can be used to predict the effect of changing the binder fluid on the drop penetration time *a priori*.

5.2. *Effect of Powder Properties on t_p*

Changing the powder properties will alter the size distribution of pores in the powder bed. This may assist or restrict fluid motion into the bed. Two approaches to investigate the effect of powder packing properties were used:

1. changing the particle size distribution to alter particle packing and pore size characteristics;

TABLE 7
Effect of Fluid Viscosity on Drop Penetration Time

Powder	Fluid	μ (mPa · s)	n	ε (−)	V_o (μL)	t_p (s)	95% CI (s)
AI ballotini	PEG200	64	23	0.49	5.7	6.9	0.6
	PEG600	153	22	0.47	5.6	17.4	1.1
UQ lactose	PEG200	64	23	0.61	5.7	9.6	0.7
	PEG600	153	21	0.59	5.7	21.7	1.1
Merck lactose	3.5% HPC	17	20	0.61	4.4	21.5	1.1
	7% HPC	103	22	0.61	4.2	123	17.7

Note. See Table 5 for nomenclature.

TABLE 8
Particle Properties of UQ Lactose and Sieved Size Fractions

Powder property	UQ lactose	UQ lactose size fraction		
		Fine	Medium	Coarse
Nominal size (μm)	150	45–106	106–180	180–250
Surface mean (μm)	64.43	32.02	48.25	69.66
Volume mean (μm)	168.7	81.61	135.46	213.25
d_{10} (μm)	38.97	26.30	33.05	45.11
d_{50} (μm)	138.2	67.18	116.68	200.22
d_{90} (μm)	348.3	145.72	255.60	387.47
$(d_{90} - d_{10})/d_{50}$	2.24	1.78	1.91	1.71
Tap density (g/mL)	0.935	0.802	0.913	0.983
Loose-packed porosity (−)	0.6	0.67	0.61	0.51
Malvern specific surface area (m^2/kg)	60.5	121.6	80.8	55.9

2. directly altering the porosity of a powder bed by using a different packing procedure.

The UQ lactose powder was sieved into three size fractions: fine (45–106 μm), medium (106–180 μm), and coarse (180–250 μm). This provided three powders with identical properties (including surface chemistry) except for particle size distribution and packing characteristics. Powder sizes and surface areas of the lactose fractions are summarized in Table 8 together with the unfractionated lactose data for comparison. Pictures of the fine and coarse fractions are shown in Fig. 12. Apart from a substantial difference in particle size and surface area, the fine fraction of lactose did not pack as well as the coarse fraction and has more angularly shaped particles. This is indicated by both the tap density and the loose packed porosity data in Table 8. The coarse fraction was more free flowing and consisted of larger, smoother, single tomahawk-shaped crystals.

The effect of particle size on penetration time can be quite dramatic. Figure 13 plots the experimental penetration times for water and PEG200 against the d_{32} particle size of the three lactose fractions. As the d_{32} size increases by a factor of 2 the penetration time decreases by a factor of 5 for PEG200 and almost a factor of 9 for water. The coarsest fraction contains larger pores which permit faster drainage and can accommodate larger volumes of liquid. In addition, the loose packing of the coarse lactose was closest to its tap density, suggesting that relatively few macrovoids were formed and that the bed structure was fairly homogeneous. The unfractionated lactose data (triangular symbols) is also shown and is in reasonable agreement with the close size fraction data. However, the size distribution of the powder must affect the penetration time as the fractionated and unfractionated results do not coincide. The powder particle size and size distribution both affect the packing and pore structure of the powder bed. The presence or absence of macrovoids in the pore space is likely to strongly affect the drop penetration time.

The majority of drop penetration experiments were performed on a very loosely packed bed to mimic as closely as possible the

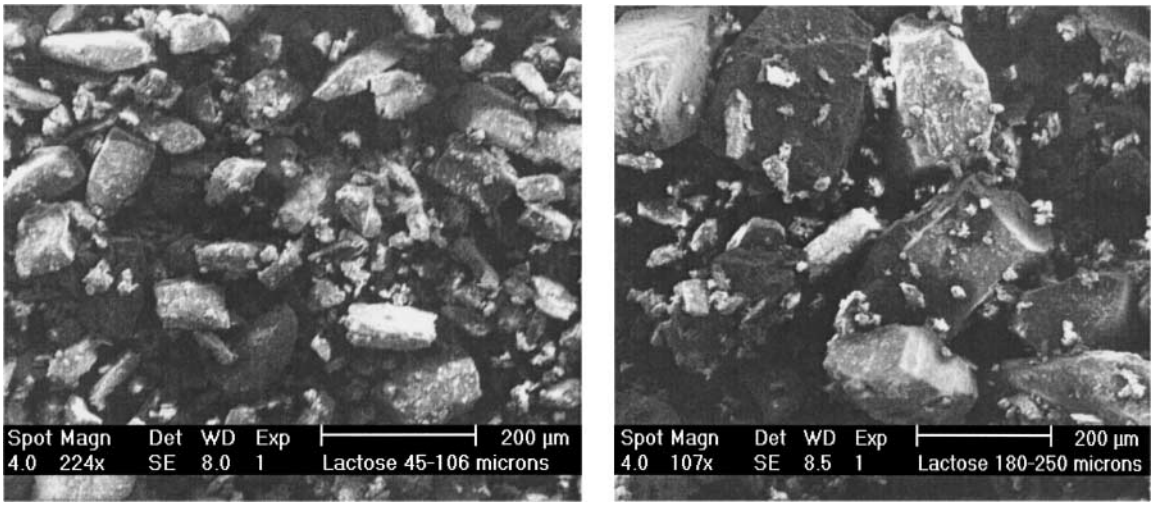

FIG. 12. SEM images of the fine (left) and coarse (right) lactose.

agitated powder conditions in a granulator. These t_p values were compared with the times obtained when the bed porosity was reduced by a combination of tapping and direct pressure using the base of a second petri dish on the powder surface. Porosity could be decreased by approximately 10% for AI ballotini and lactose.

Loosely poured beds contain many local "bubble void" regions of extremely low density which collapse readily when disturbed (9). Tapping or light pressure on the surface of a loosely packed powder bed resulted in settling and compaction of the powder bed. These dishes were handled very gently.

Table 9 summarizes the porosity, the Hausner ratio H, and the penetration time results for AI ballotini and UQ lactose. Although both powders have almost identical values of ε_{tap}, their loose packing configurations are quite different. The ballotini powder always packs quite close to its minimum tapped porosity, as the Hausner ratios are always close to unity irrespective of whether the ballotini powder bed is prepared by "loose" or "firm" packing conditions. However, UQ lactose are irregular crystal shapes and are able to sustain much larger void space (approximately 60%) within their loose packing arrangement. This is reflected in the H ratios of 1.6 and 1.3 for loose and firm packing conditions respectively. Substantial tapping was required to rearrange the particles and reduce the voidage. This was also observed when preparing the small column of powder for contact angle measurements.

Table 9 shows no clear trend between ε and t_p. From Eq. [9] the penetration time should decrease in proportion to ε^2, assuming that the powder pore size remains constant. In practice, R_{pore} and

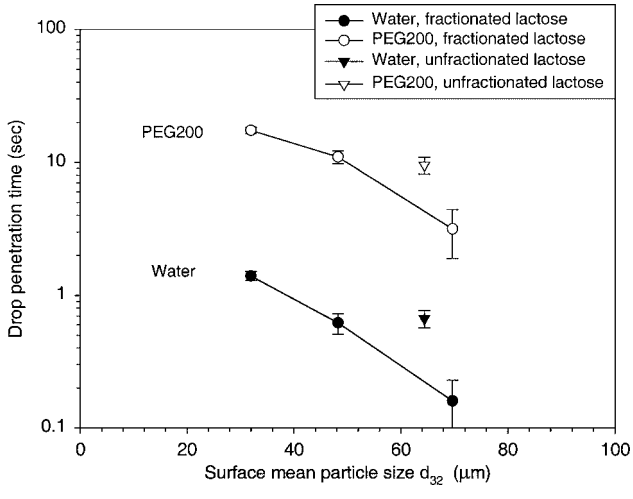

FIG. 13. Effect of d_{32} particle size on penetration time. Circles represent the mean result of several experiments on fine, medium, and coarse UQ lactose powder and error bars show 95% confidence interval. Triangles represent the same fluid on the unfractionated lactose.

TABLE 9
Effects of Bed Porosity on Drop Penetration Times

Powder	Fluid	n	ε (−)	H (−)	V_o (μL)	t_p (s)	95% CI (s)
AI ballotini	Water	20	0.45	1.2	11.6	0.63	0.04
$\varepsilon_{tap} = 0.390$		20	0.42	1.1	8.5	0.45	0.06
	PEG200	23	0.49	1.2	5.7	6.9	0.6
		21	0.43	1.1	5.5	5.8	0.4
	PEG600	22	0.47	1.2	5.6	17.4	1.1
		20	0.40	1.0	5.7	18.6	2.7
UQ lactose	Water	21	0.61	1.6	9.0	0.67	0.05
$\varepsilon_{tap} = 0.392$		18	0.50	1.3	10.0	0.56	0.05
	PEG200	23	0.61	1.6	5.7	9.6	0.7
		20	0.48	1.2	6.3	10.7	0.9
	PEG600	21	0.59	1.5	5.7	21.7	1.1
		20	0.49	1.3	6.0	27.5	2.4

Note. See Table 5 for nomenclature.

ε are intimately connected and it is difficult to vary one without altering the other. The effect of ε on t_p depends on the particular powder and fluid used. In general, t_p changes only slightly when the porosity of a glass ballotini powder bed is reduced, but it is affected by ε on lactose powder which has a much higher Hausner ratio. The effect of porosity on penetration time cannot be evaluated without considering pore size.

6. COMPARISON WITH THEORY

Three equations for calculating R_{pore} have been presented and there are five possible methods of estimating R_{pore}:

1. Eq. [3] with S_o equal to the particle specific surface area measured by BET;
2. Eq. [3] with S_o equal to the particle specific surface area measured by Malvern laser diffraction;
3. Eq. [3] with S_o equal to the wetted specific surface area measured during contact angle analysis;
4. Eq. [4] using Malvern measured surface mean size d_{32};
5. Eq. [8] using effective porosity ε_{eff} and effective pore size R_{eff} equations for loosely packed powder beds.

Table 10 compares the porosities, effective porosities, and the pore size estimates by these different methods.

The pore size estimation method affects the estimated value of R_{pore} as illustrated in Table 10. The BET method estimates much finer pores that the other methods and the wetted surface area method predicts the largest pores.

The estimated pore size using the surface mean size d_{32} and the Malvern specific surface area are almost identical. This is not surprising since both were measured by laser diffraction. The Malvern d_{32} size will be used instead of the specific surface area in the remainder of this work as the results are virtually identical.

Calculations of the effective porosity gives $\varepsilon_{eff} \approx 0.3$ for all powders. This in turn leads to much smaller estimated pore sizes using the new theory when compared to the standard Kozeny approach. Pore sizes are reduced by a factor of between 1 and 2 for ballotini, 2 and 4 for lactose powder, and by an order of magnitude for the finest powders.

To differentiate between the various methods of estimating R_{pore}, the measured penetration times need to be compared with the theoretically predicted times.

6.1. Comparison of Theoretical and Experimental t_p

Decreasing drawing area behavior was not observed for any powder/fluid combination used in this work. Therefore, advancing and receding contact angles must be considered when

TABLE 10
Comparison of R_{pore} Estimation Methods

Powder	Fluid	d_{32} (mm)	ε (−)	ε_{tap} (−)	$\varepsilon_{macrovoids} = \varepsilon - \varepsilon_{tap}$	ε_{eff} (−)	Kozeny R_{proe} (μm) BET S_o	Malvern S_o	Wetted SA	d_{32}	R_{eff} (μm)
AI ballotini	Water	29.6	0.45	0.39	0.06	0.37	4.2	8.3	10.2	8.1	5.8
	PEG200	29.6	0.49	0.39	0.09	0.35	4.9	9.6	11.8	9.3	5.4
	PEG600	29.6	0.47	0.39	0.08	0.36	4.5	8.9	11.0	8.7	5.6
	NDBS	29.6	0.52	0.39	0.13	0.34	5.5	11.0	13.4	10.6	5.1
	Water	29.6	0.42	0.39	0.03	0.38	3.8	7.5	9.2	7.3	6.0
	PEG200	29.6	0.43	0.39	0.03	0.38	3.8	7.6	9.4	7.4	6.0
	PEG600	29.6	0.40	0.39	0.01	0.39	3.5	6.9	8.5	6.7	6.2
AE	PEG200	113.9	0.38	0.39	0.0	0.38	5.7	23.5	30.6	22.8	22.7
Lactose	Water	64.4	0.61	0.39	0.21	0.31	—	33.0	40.0	33.0	9.5
	PEG200	64.4	0.61	0.39	0.22	0.31	—	33.2	40.2	33.1	9.5
	PEG600	64.4	0.59	0.39	0.2	0.31	—	30.8	37.3	30.7	9.8
	NDBS	64.4	0.63	0.39	0.24	0.30	—	36.9	44.7	36.8	9.1
	Satd Soln	64.4	0.55	0.39	0.16	0.33	—	26.6	32.2	26.5	10.5
	Water	64.4	0.50	0.39	0.11	0.35	—	21.2	25.7	21.2	11.6
	PEG200	64.4	0.48	0.39	0.09	0.35	—	20.3	24.5	20.2	11.8
	PEG600	64.4	0.49	0.39	0.10	0.35	—	20.9	25.3	20.9	11.6
Fine	Water	32.0	0.66	0.48	0.18	0.39	—	21.0	—	21.0	6.8
	PEG200	32.0	0.68	0.48	0.20	0.38	—	22.3	—	22.2	6.6
Medium	Water	48.3	0.61	0.41	0.21	0.32	—	25.6	—	25.6	7.6
	PEG200	48.3	0.61	0.41	0.20	0.32	—	25.1	—	25.0	7.7
Coarse	Water	69.7	0.50	0.36	0.14	0.31	—	23.3	—	23.2	10.4
	PEG200	69.7	0.52	0.36	0.16	0.30	—	25.0	—	25.0	10.1
ZnO	Water	1.25	0.92	0.6	0.32	0.41	0.83	4.6	—	4.6	0.3
	PEG200	1.25	0.92	0.6	0.32	0.41	0.82	4.5	—	4.5	0.3
TiO_2	PEG200	0.73	0.84	0.6	0.24	0.46	1.6	1.27	—	1.27	0.2

TABLE 11
Comparison of Drop Penetration Times

Powder	Fluid	τ_{CDA} BET	τ_{CDA} Wetted SA	τ_{CDA} d_{32}	τ_{CDA} R_{eff} and ε_{eff}	t_p (s)	95% CI (s)
AI ballotini	Water	**0.20**	0.08	0.11	0.15	**0.63**	0.04
	PEG200	13.2	5.7	**6.8**	11.7	**6.9**	0.6
	PEG600	40.7	**16.5**	20.9	32.5	**17.4**	1.1
	NDBS	—	0.08	0.10	**0.21**	**0.65**	0.09
	Water	**0.21**	0.08	0.11	0.13	**0.45**	0.06
	PEG200	20.8	**8.5**	10.7	13.3	**5.8**	0.4
	PEG600	71.7	**29.1**	36.8	39.8	**18.6**	2.7
AE	PEG200	21.3	**3.1**	4.2	4.2	**3.0**	0.2
Lactose	Water	—	0.01	0.02	**0.22**	**0.67**	0.05
	PEG200	—	1.0	1.2	**16.0**	**9.6**	0.7
	PEG600	—	2.7	3.2	**35.3**	**21.7**	1.1
	NDBS	—	0.02	0.01	**0.20**	**0.72**	0.1
	Satd Soln	—	0.02	0.05	**0.36**	**0.61**	0.07
	Water	—	0.03	0.04	**0.15**	**0.56**	0.05
	PEG200	—	2.7	3.3	**10.4**	**10.7**	0.9
	PEG600	—	5.8	7.0	**24.8**	**27.5**	2.4
Fine	Water	—	—	0.02	**0.21**	**1.4**	0.09
	PEG200	—	—	1.4	**14.5**	**17.4**	0.7
Medium	Water	—	—	0.02	**0.26**	**0.62**	0.09
	PEG200	—	—	1.6	**18.4**	**11.0**	0.9
Coarse	Water	—	—	0.04	**0.21**	**0.16**	0.06
	PEG200	—	—	**2.3**	16.37	**3.2**	1.00
Merck lactose	Water	—	—	0.03	**0.27**	**2.0**	0.3
	3.5% HPC	—	—	0.52	**6.51**	**21.5**	1.1
	7% HPC	—	—	3.3	**47.5**	**126**	23
ZnO	Water	**0.13**	—	0.02	2.2	**0.6**	0.15
	PEG	**10.5**	—	0.02	1.7	**19.7**	4.4
TiO_2	PEG200	0.12	—	0.16	**3.3**	**8.7**	1.6

describing drop penetration into powder beds. The constant drawing area method (Eq. [1]) will be used to calculate the drop penetration time and evaluate the best method of estimating the powder pore size. The τ_{CDA} prediction are summarized in Table 11 together with the experimental times. The closest prediction of the penetration time is highlighted in gray.

Table 11 shows that using the BET surface area to estimate powder pore size is inaccurate. The smaller pore sizes lead to large overrestimates of penetration time for ballotini and lactose. The exception is the fine ZnO powder, where the BET method is most accurate. The difficulty of measuring the BET surface area of common powders such as lactose make this a poor choice for characterizing pores. The d_{32} and wetted surface areas perform equally well in predicting the penetration time on glass ballotini, and generally predict τ_{CDA} values within a few seconds of the measured times (see Fig. 14). Since the d_{32} is a simple parameter to measure it is the most preferable choice for estimating R_{pore}.

Figure 14 compares the ballotini and lactose τ_{CDA} predictions from Eqs. [1] and [4] (6, 7) with the experimental results. If the model is correct the data should be scattered around the solid equality line or at least within the dashed lines which represent

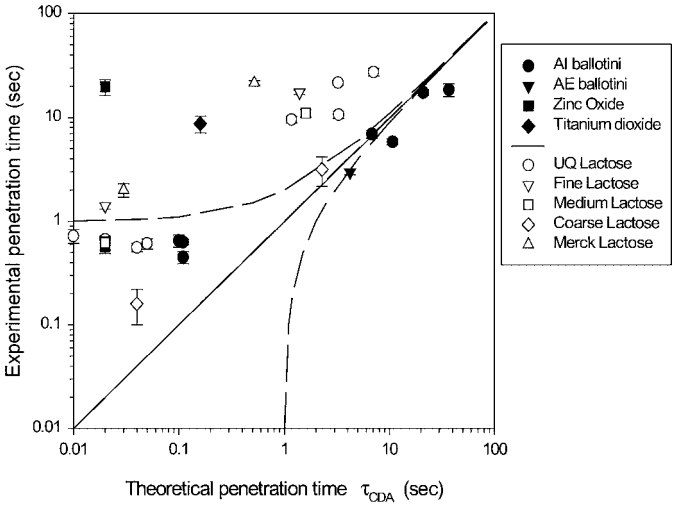

FIG. 14. Experimental vs theoretical penetration times. Theoretical times calculated using Kozeny approach R_{pore} with d_{32} from Malvern (Eq. [4]). Solid line is the equality line and the dashed lines show ±1 s.

±1 s. The existing drop penetration time model with the Kozeny approach to pore size works well for glass ballotini powders. Ballotini powers have very low Hausner ratios and were expected to follow the Kozeny approach as macrovoids are unlikely to form in the pore structure. However, the existing methods perform very poorly on lactose, ZnO and TiO_2 powders. The experimental penetration times are an order of magnitude larger than the t_p predictions from Eqs. [1] and [4].

Figure 15 compares the new theory from Eqs. [7] to [9] with the experimental penetration times. The improved theory performs adequately with all powders and greatly improves the lactose powder results. Most of the data are scattered around the equality line and within ±1 s of the penetration time. The improved theory is much better at predicting penetration times on

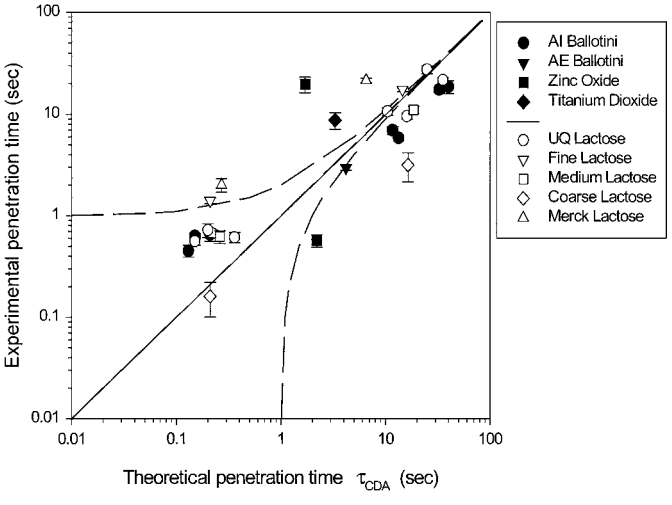

FIG. 15. Experimental drop penetration times versus the times predicted by the improved theory with ε_{eff} and R_{eff} in Eqs. [7] to [10]. Solid line is the equality line and the dashed lines show ±1 s.

loosely packed powders and allows t_p to be predicted within an order of magnitude for all powders except for ZnO and TiO_2. These powders are much finer and very cohesive and are expected to have a much more complex microstructure. Equations [7] to [9] are crude estimates of effective porosity and pore size in loosely packed beds and there is considerable scope for improvement.

The kinetics of penetration is too complex to depend only on R_{pore} and ε_{eff}. In substrates with heterogeneous pore distributions, unsaturated flow occurs as the liquid redistributes into the smaller pores (9, 27, 32). Drop penetration and unsaturated spreading of the fluid are likely to occur in parallel where there is a limited reservoir of fluid. Other complicating factors which affect the interfacial driving force include (but are not limited to) the effect of dynamic contact angle (6, 33), dissolution of the substrate during penetration, inertia of the fluid during penetration (6), displacement of the air in the pores (6, 10) and adsorption of solutes onto the substrate surface. This can make contact angle and effective pore size measurements difficult to interpret. These phenomena are complex and deserve future research. Notwithstanding these effects, the simple method of incorporating the effect of macrovoids in loose packed powder beds greatly improves the accuracy of drop penetration time predictions.

7. SUMMARY

Drop penetration times have been shown to range over several orders of magnitude and that the actual time taken for the liquid to be incorporated within the bed structure is much longer than previously thought (6, 7). This work confirms that the drop penetration behavior on loosely packed porous powder beds is quite complex and highly dependent on the microstructure of the bed. The heterogeneous structure of loosely packed powder beds and the presence of macrovoids must be considered when studying liquid imbibition where the only driving force is capillary pressure. Under these conditions the macrovoids do not participate in liquid flow and additionally inhibit the path of the liquid. Traditional methods of estimating pore size (Kozeny equation) inherently include the macrovoids and from a permeability standpoint, the presence of macrovoids should assist liquid flow.

After recalculating the pore size and penetration times using the effective porosity, the model presented here was much more successful at estimating t_p on a range of different powders and the predicted times were generally within an order of magnitude of the experimental results. Further research on liquid drainage in heterogeneous powder beds is required.

Ideal nucleation conditions and short penetration times are assisted by small drops, low-viscosity fluids, porous powders (but without macrovoids), large powder pores, high surface tension, and low contact angle.

ACKNOWLEDGMENTS

Thanks to Research Officer David Page for his assistance with particle characterization and the Chemistry Department at the University of Newcastle for use of the contact angle apparatus. This work was funded by the University of Queensland, the UQ Department of Chemical Engineering, Merck & Co. Inc., and the International Fine Particle Research Institute.

REFERENCES

1. Ennis, B. J., and Litster, J. D., *in* "Perry's Chemical Engineers' Handbook" (D. Green, Ed.), McGraw-Hill, New York, 1997.
2. Litster, J. D., Hapgood, K. P., Michaels, J. N., Kamineni, S. K., Hsu, T., Sims, A., and Roberts, M., *Powder Technol.* **114,** 32 (2001).
3. Link, K. C., and Schlünder, E.-U., *Chem. Eng. Technol.* **19,** 432 (1996).
4. Hunter, R. J., "Foundations of Colloid Science," Oxford Univ. Press, Oxford, 1986.
5. Popovich, L., Feke, D. L., and Manas-Zloczower, I., *Powder Technol.* **104,** 68 (1999).
6. Middleman, S., "Modeling Axisymmetric Flows: Dynamics of Films, Jets, and Drops," Academic Press, San Diego, 1995.
7. Denesuk, M., Smith, G. L., Zelinski, B. J. J., Kreidl, N. J., and Uhlmann, D. R., *J. Colloid Interface Sci.* **158,** 114 (1993).
8. Marmur, A., *J. Colloid Interface Sci.* **124,** 301 (1988).
9. Marmur, A., and Cohen, R. D., *J. Colloid Interface Sci.* **189,** 299 (1997).
10. Dullien, F. A. L., *in* "Handbook of Powder Science and Technology" (M. E. Fayed and L. Otten, Eds.), Vol. 1, p. 53, Chapman and Hall, New York, 1997.
11. Kaye, B. H., "Characterization of Powders and Mists," Wiley-VCH, Weinheim, 1999.
12. Hausner, H. H., *Int. J. Powder Metall.* **4,** 7 (1967).
13. Davidson, J. F., and Harrison, O., "Fluidization," Academic Press, London and New York, 1971.
14. Berlin, E., Anderson, B. A., and Pallansch, M. J., *J. Dairy Sci.* **55,** 1396 (1972).
15. Iveson, S. M., "Fundamental Studies of Granulation: Granule Deformation and Consolidation," Ph.D. thesis, University of Queensland, 1997.
16. White, L. R., *J. Colloid Interface Sci.* **90,** 536 (1982).
17. Diggins, D., Fokkink, L. G. J., and Ralston, J., *Colloids Surf.* **44,** 299 (1990).
18. Prestige, C. A., and Ralston, J., *J. Colloid Interface Sci.* **172,** 302 (1995).
19. Iveson, S. M., Holt, S., and Biggs, S., *Colloids Surf. A* **166,** 203 (1999).
20. Jaiyeoba, K. T., and Spring, M. S., *J. Pharm. Pharmacol.* **32,** 386 (1980).
21. Lerk, C. F., Schoonen, A. J. M., and Fell, J. T., *J. Pharm. Sci.* **65,** 843 (1976).
22. Pepin, X., Blanchon, S., and Couarraze, G., *Powder Technol.* **99,** 264 (1998).
23. Kiesvaara, J., and Yliruusi, J., *Int. J. Pharm.* **92,** 81 (1993).
24. Dunstan, D., and White, L. R., *J. Colloid Interface Sci.* **111,** 60 (1986).
25. Mackaplow, M. B., Rosen, L. A., and Michaels, J. N., *Powder Tech.* **108,** 32 (2000).
26. Huethorst, J. A. M., and Leenars, A. F. M., *Colloids Surf.* **50,** 101 (1990).
27. Schaafsma, S. H., Vonk, P., Segers, P., and Kossen, N. W. F., *Powder Technol.* **97,** 183 (1998).
28. Aulton, M. E., and Banks, M., "Influence of the Hydrophobicity of the Powder Mix on Fluidised Bed Granulation," International Conference on Powder Technology in Pharmacy, Basel, Switzerland Powder Advisory Centre, 1979.
29. Danjo, K., Kamiya, A., Ikeda, E., Sunda, H., and Otsuka, A., *Chem. Pharm. Bull.* **40,** 2505 (1992).
30. Durán, J. D. G., Delgado, A. V., and González-Caballero, *Mater. Chem. Phys.* **38,** 42 (1994).
31. Crowl, V. T., and Woolridge, W. D. S., *in* "Wetting," Soc. Chem. Ind., 1967.
32. Danino, D., and Marmur, A., *J. Colloid Interface Sci.* **166,** 245 (1994).
33. Siebold, A., Nardin, M., Schultz, J., Wallizer, A., and Oppliger, M., *Colloids Surf. A* **161,** 81 (2000).